III International Conference on Particle-based Methods – Fundamentals and Applications
PARTICLES 2013
M. Bischoff, E. Oñate, D.R.J. Owen, E. Ramm & P. Wriggers (Eds)

A DEM STUDY OF SILO DISCHARGE OF A COHESIVE SOLID

J.P. MORRISSEY[1], J.Y. OOI[1] AND J.F. CHEN[2]

[1] Institute for Infrastructure and Environment, School of Engineering,
The University of Edinburgh, EH9 3JL, Scotland, U.K
E-mail: j.ooi@ed.ac.uk

[2] School of Planning, Architecture and Civil Engineering, Queen's University Belfast,
Belfast BT9 5AG, Northern Ireland, UK

Key words: Granular Materials, DEM, Cohesion, Silo Discharge.

Abstract. Bulk handling of powders and granular solids is common in many industries and often gives rise to handling difficulties especially when the material exhibits complex cohesive behaviour. For example, high storage stresses in a silo can lead to high cohesive strength of the stored solid, which may in turn cause blockages such as ratholing or arching near the outlet during discharge.

This paper presents a Discrete Element Method study of discharge of a granular solid with varying levels of cohesion from a flat-bottomed silo. The DEM simulations were conducted using the commercial EDEM code with a recently developed DEM contact model for cohesive solids implemented through an API. The contact model is based on an elasto-plastic contact with adhesion and uses hysteretic non-linear loading and unloading paths to model the elastic-plastic contact deformation. The adhesion parameter is a function of the maximum contact overlap. The model has been shown to be able to predict the stress history dependent behaviour depicted by a flow function of the material.

The effects of cohesion on the discharge rate and flow pattern in the silo are investigated. The predicted discharge rates are compared for the varying levels of cohesion and the effect of adhesion is evaluated. The ability of the contact model to qualitatively predict the phenomena that are present in the discharge of a silo has been shown with the salient feature of mixed flow from a flat bottomed hopper identified in the simulation.

1 INTRODUCTION

A recently developed Elasto-Plastic Adhesive contact model is used to carry out DEM simulations of a flat bottomed silo during discharge across a spectrum of adhesion energy values. The level of adhesion in the system is increased incrementally for cohesionless, mild, moderate, sever and extreme levels of cohesion in an assembly. This study serves as an exploration of the effect of adhesive forces of the discharge process and an assessment of the capability of the contact model to qualitatively predict the phenomena that are present in the discharge of a silo. A flat bottomed silo has been chosen due to its simplicity and ease of comparison to theories such as Beverloo's discharge theory.

2 DEM IMPLEMENTATION

A DEM contact model based on an elasto-plastic model with adhesion [1–3] which includes hysteretic linear and non-linear loading paths [4] is adopted. The DEM contact model is based on the physical phenomena observed in adhesive contact experiments [5]. When two particles or agglomerates are pressed together, they undergo elastic and plastic deformations and the pull-off (adhesive) force increases with an increase of the plastic contact area.

2.1 Contact Model

A non-linear contact model that accounts for both the elastic-plastic contact deformation and the contact-area dependent adhesion is presented. The schematic diagram of particle contact and normal force-overlap (f_n- δ) for this model is shown in Figure 1.

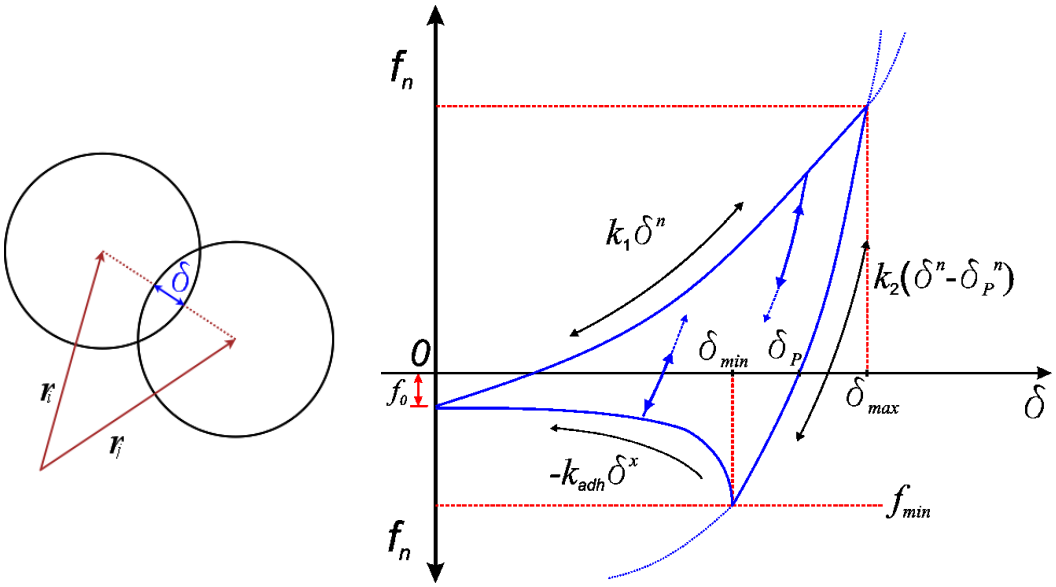

Figure 1 - Normal Force-Overlap Relationship for EEPA Contact model

The normal contact force-overlap relationship may be mathematically expressed by equation 1, which includes a constant attractive force f_0 that can be used to account for the effect of van der Waals type forces is considered. The loading, unloading/re-loading, and adhesive branches are characterised by six parameters: the virgin loading stiffness parameter k_1, the unloading and reloading stiffness parameter k_2, the constant adhesion force f_0, the stiffness exponent n, the adhesion path exponent x and the and the contact surface energy Δγ. The shape of all the three branches is controlled by the parameters n and X – they all become linear at an exponent value of unity [6], [7]. Furthermore, if k_1 is set equal to k_2 the model is reduced to an elastic contact model. Upon reloading, the contact force initially follows along the reloading k_2 path but switches to the virgin loading k_1 path when the previous maximum loading force is reached. Unloading below the plastic overlap δ_p results in the development of an attractive force until the maximum attractive force f_{min} is reached at δ_{min}.

$$f_{hys} = \begin{cases} f_0 + k_1\delta^n & if\ k_2\left(\delta^n - \delta_p^n\right) \geq k_1\delta^n \quad (a) \\ f_0 + k_2\left(\delta^n - \delta_p^n\right) & if\ k_1\delta^n > k_2\left(\delta^n - \delta_p^n\right) > -k_{adh}\delta^x \quad (b) \\ f_0 - k_{adh}\delta^x & if\ -k_{adh}\delta^x \geq k_2\left(\delta^n - \delta_p^n\right) \quad (c) \end{cases} \quad \textbf{(1)}$$

Further unloading past this point results in a reduction in both the normal overlap and the attractive force until separation occurs. In this study a value of n=1.5 has been used. The tangential force is calculated using the Mindlin tangential contact model.

2.2 DEM Model Setup

In this study each particle is formed by two overlapping spheres with an aspect ratio of 1.5 to better represent a real granular solid. Each sphere has a radius of 2mm, giving a multi-sphere particle 4mm x 6mm in size. Particle-particle friction has been set to a value of 0.5 as low friction values of less than approximately 0.2 lead to the situation where discharge rates becomes dependent of the fill height of the assembly. Particle-wall friction has been set to a median value of 0.5. The coefficient of restitution has been observed to have negligible effect on silo discharge and a value of 0.5 has been selected.

The model consists of a periodic slice. Experience shows that a sufficiently large depth is required to produce stable results, so a thickness of between 4-6 particle diameters is used. In order to avoid any mechanical arching around the outlet, an opening width of approximately 12-15 particle diameters has been utilised. The ratio of the opening width to the total silo width has been set at 0.2. The final model silo dimensions are 0.8m tall by 0.3m wide with a depth of 0.025m between the two periodic boundaries. An opening width of 0.06m is located centrally for the whole depth of the slice. The number of particles used to fill the model silo is slightly under 61,000 after the top surface has been levelled by removing some particles.

The filling of the sample took place using a centrally located dynamic factory that filled the assembly under normal gravity over a period of 1.5s before settling for a further 1s. The sample was initially filled in the absence of any cohesion. The same assembly of particles was then used with varying levels of adhesion energy to avoid any effects that may develop from different assemblies. Implementing a gravity fill method allows a more realistic packing structure to be formed than an *en-masse* generation scheme which places all particles at once and can hinder the arching and development of friction that is necessary to successfully predict the real behaviour. The full set of parameter used for the simulations are given in Table 1. A simulation timestep of 5×10^{-06} s, which is approximately $0.075\sqrt{m/k}$ was adopted in all simulations. Data were recorded for each simulation at a rate of 100Hz.

Table 1 - Simulation Parameters

Particle Radius, R (m)	0.002	Poisson's Ratio, ν	0.25
Particle Aspect Ratio, AR_p	1.5	Adhesion Energy, Δγ (J/m^2)	0, 5,10,12.5,15
Particle Density, ρ (kg/m^3)	5400	Particle Sliding Friction, μ_s	0.5
Young's Modulus, E (Pa)	1.25E+08	Particle Rolling Friction, μ_r	0.005
Shear Modulus, G (Pa)	5E+07	Wall Friction, μ_w	0.5
Spring Stiffness, k_1 (N/m)	3.0E+06	Base Friction, μ_b	0.5
Spring Stiffness, k_2 (N/m)	7.5E+07	Simulation Time step (s)	5E-06

3 SILO DISCHARGE

When discharge commences by opening the outlet a mixed mode of flow can be seen in Fig. 2. In the upper section of the silo the flow mode is mainly mass flow, whereas due to the flat bottom a flow channel develops from the opening at approximately 45 degrees towards the silo walls.

Studies carried out by Munch-Andersen [8] using grains found that a boundary layer of particles is observed near the silo wall during discharge. The thickness of the layer observed varies with the roughness of the wall, with rougher more frictional surfaces leading to a thicker layer. A detailed experimental study on the discharge of sand from a silo also documented the same effect [9].

The boundary effect of wall friction is also seen in the DEM simulation results, in which a layer of slow moving particles approximately 5-10 particles thick exists. Due to the larger particle size of the DEM particles the effect, is more obvious but displays the same trends as seen in experiments, with the formation of a bank starting to develop in Figure 2(b) and more prominent in Figure 2(c). The surface profile remains relatively unchanged initially, but as the simulation progresses, the effect of the faster flow in the centre leaves a more pronounced dip in the centre of the surface profile, similar to what was reported by Munch-Andersen [9]. Throughout discharge there is a stagnant zone on each side of the outlet which remains after discharge ends. The features found in the DEM simulations are also well described by the kinematic model for solid flow in flat bottomed hoppers by Zhang & Ooi [10].

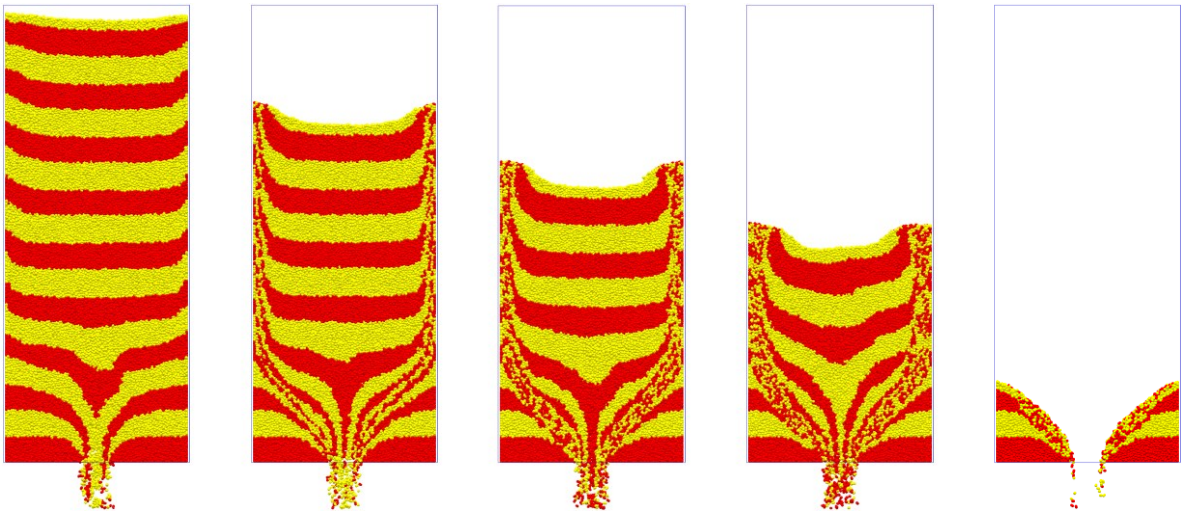

Figure 2 - Discharge for cohesionless particles

The effect of cohesion on discharge is depicted in Figure 3 at T=1s. In the cohesionless assembly in Figure 3(a) the material is free flowing in all areas of the silo except the two stagnant zones at the bottom, while mass flow has developed in the upper section of the silo. As the adhesion increases and the material becomes mildly (Figure 3(b)), and moderately cohesive (Figure 3(c)), the discharge rate is reduced and this leads to slower development of the funnel flow channel which has been restricted to an area directly over the outlet at this stage of discharge. Some intermittent arching is noted for the moderately cohesive assembly

during discharge and almost no flow is noticed in the upper section of the silo after 1 second (Figure 3(c)).

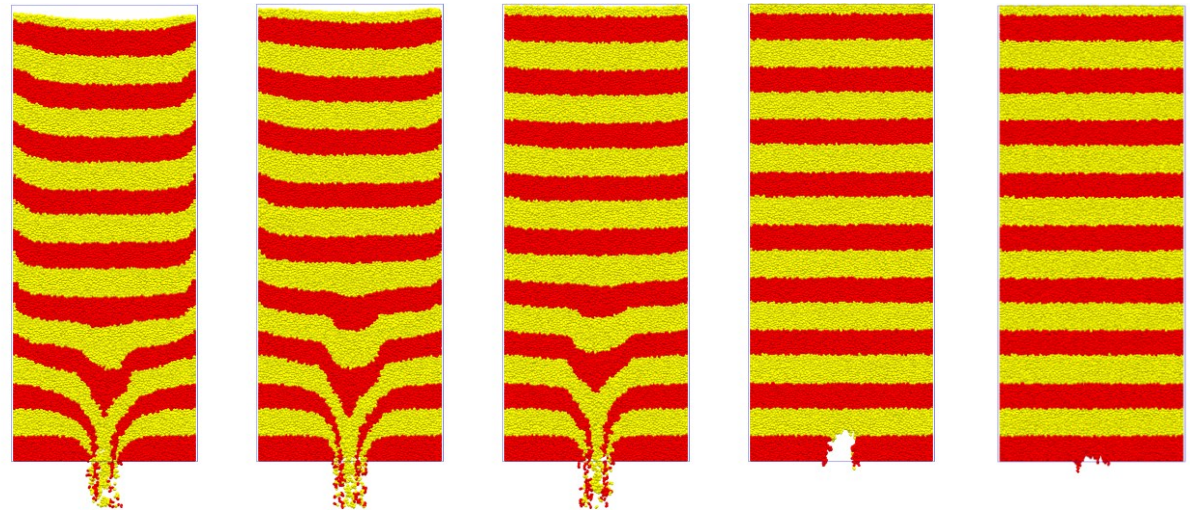

Figure 3 - Discharge for various cohesion values at T = 1s

For a strongly cohesive assembly (Figure 3(d)), there is significant intermittent arching across the outlet, which leads to a blockage that lasts for more than 0.5 seconds. While further intermittent cohesive arching occurs it is not enough to prevent discharge. In an extremely cohesive assembly, such as Figure 3(e), a permanent cohesive arch forms and prevents any flow from the silo.

3.1 Discharge Rates

The discharge rate was investigated for the varying levels of adhesion during the discharge process for the flat bottomed hopper. In the case of cohesionless flow; as the flow from the silo is mixed funnel flow; the widely used Beverloo model [11] can be applied to compare the theoretical discharge rate with that predicted from the DEM simulation. The modified Beverloo equation for rectangular silo with a rectangular slot proposed by Myers & Sellers [12] was used. As non-spherical particles with an aspect ratio of 1.5 have been used, the Beverloo coefficient k has been set as 1.65 with the initial bulk density for the silo found to be 3310 kg/m^3, leading to a Beverloo discharge rate of 1 kg/s.

The temporally averaged DEM mass flow rates for all levels of adhesion energy, $\Delta\gamma$, are presented in Figure 4. The average mass flow rates for discharge and the mass flow velocities, $V_{MF,}$ for different adhesion energy values are given in Table 2. The temporally averaged discharge rate is found to be quite stable with only small fluctuations during discharge until the silo is almost empty, at which point the discharge rate begins to drop. The DEM prediction is in excellent agreement with the Beverloo prediction for the cohesionless discharge with only 2% difference.

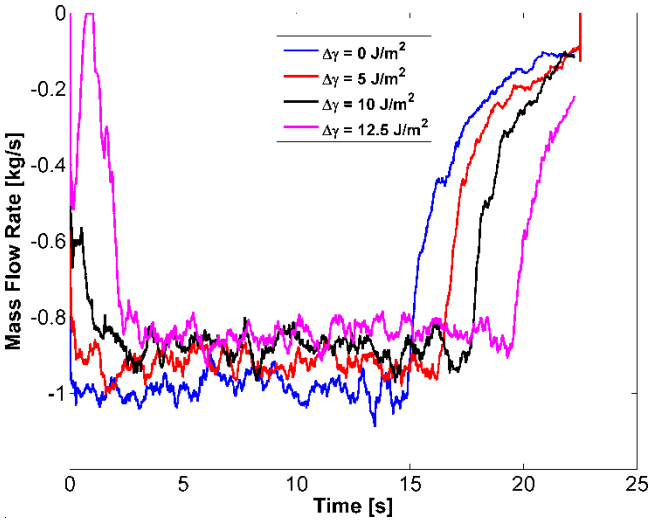

Figure 4 - Discharge rates averaged temporally over 0.5s

Table 2 - Discharge Rates

Adhesion Energy, Δγ [J/m^2]	Mass Flow Rate [kg/s]	Mass flow Velocity, V_{MF} [m/s]
0	0.98	0.039
5	0.92	0.037
10	0.88	0.035
12.5	0.84	0.034

Although there are fluctuations to be found in the discharge rate a general trend of reducing discharges rates with increasing adhesion can be found from the DEM simulations. The reduction in discharge rate leads to a longer total discharge time for the simulations. And while the lower discharge rates contribute to the longer discharge times, a significant portion of the extra time also comes from intermittent arching at the initial stages of flow. This is particularly evident for moderately and strongly cohesive assemblies, where a stable discharge rate is not reached until approximately two seconds into discharge compared to approximately 0.2s for the cohesionless case. For the strongly cohesive assembly a significant arch develops after approximately 0.25s which reduces discharge to zero for more than half a second. The effects of smaller intermittent arches are also seen in the moderately cohesive assembly but these are not significant enough to stop discharge completely.

4 VELOCITY PROFILES AND FLOW MODES

4.1 Velocity Profiles

The velocity profiles at selected vertical locations in the silo are presented for both the cohesionless assembly and strongly cohesive assembly, for a selection of time steps during discharge (Figure 5 and Figure 6). Velocity profiles were extracted from the analysed simulations which were temporally averaged with a sampling frequency of 10 Hz. In all cases a peak velocity was noted centrally above the silo outlet. A reduced velocity was also noted in the boundary layer at the edge of the silo. Mass flow was observed in the upper section of the silo.

A constant discharge rate was found in the cohesionless assembly from approximately T= 0.5s onwards whereas a stable discharge rate was not observed in the strongly cohesive assembly until approximately T= 3s. In Figure 5(a) the velocity profiles for the cohesionless assembly are presented. Mass flow with a velocity equal to V_{MF} from Table 2 is observed above a height-to-width (H/W) ratio of approximately 0.75. This height can be observed as

the effective transition, below which height funnel flow is experienced, with a high velocity core flow channel occurring directly over the silo outlet. A similar flow pattern is observed for the strongly cohesive assembly, although mass flow has not yet developed in this assembly at T= 2.5s.

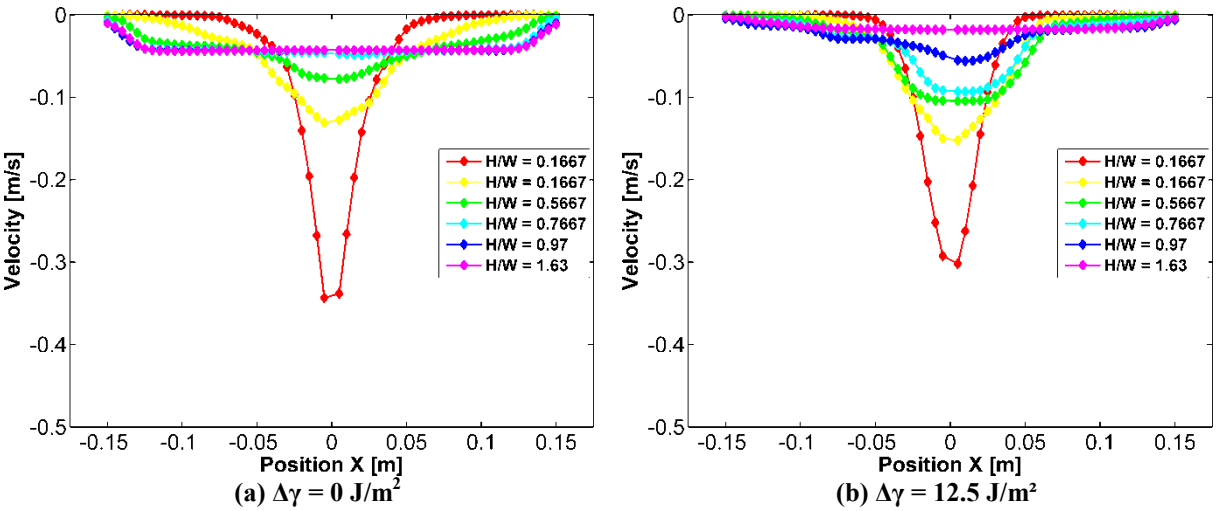

(a) $\Delta\gamma = 0$ J/m^2 (b) $\Delta\gamma = 12.5$ J/m²

Figure 5 - Velocity profiles at T = 2.5s

By T= 5s, however, stable discharge with mass flow and the same characteristics as the cohesionless assembly have developed for the strongly cohesive assembly. The addition of adhesion to the system has not led to a change in the flow mode predicted in the DEM simulation; however it has led to reduced velocities and discharge rates.

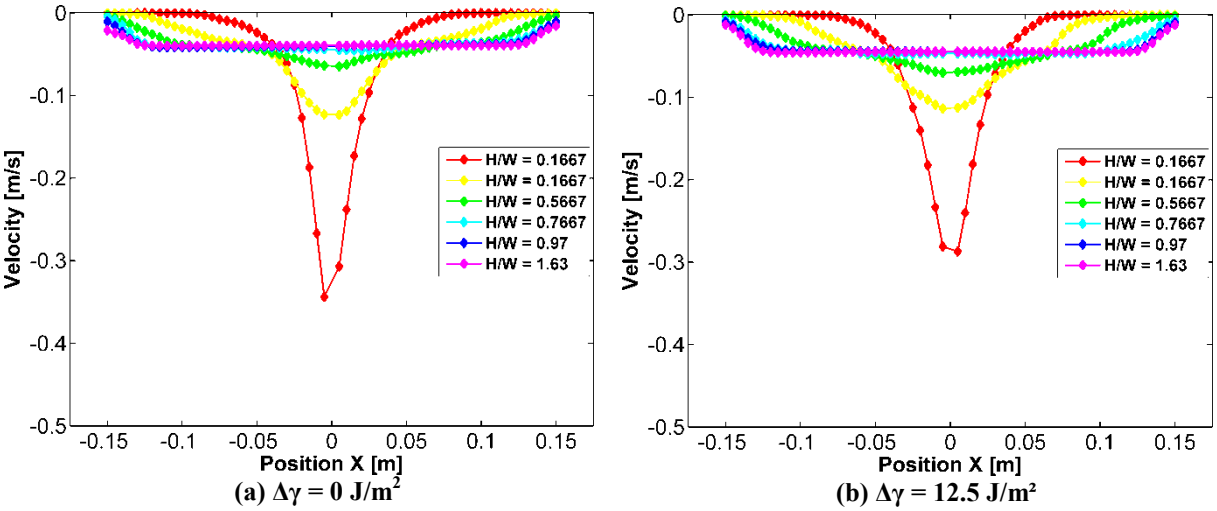

(a) $\Delta\gamma = 0$ J/m^2 (b) $\Delta\gamma = 12.5$ J/m²

Figure 6 - Velocity profiles at T = 5s

4.2 Flow Channels

The observed flow channel in the silo for the cohesionless assembly is displayed in Figure

7. In Figure **7**a the limits of the flow zone have been defined with a velocity of 0.005 m/s which highlights the areas of shearing between the stagnant zone and the flowing material. The effective transition height, where the flow boundary meets the silo wall at between H/W = 0.75-0.8, is also clearly visible with some asymmetry in the flow being noted. Adopting a minimum velocity of 1.25 V_{MF} (Figure **7**b) highlights the high velocity core flow zone.

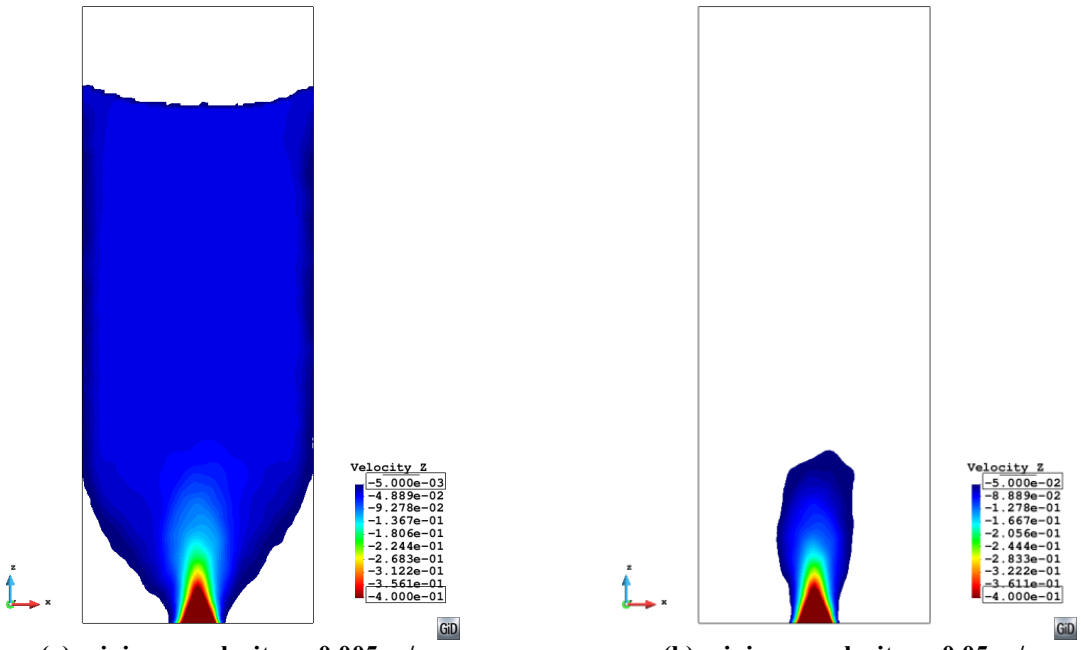

(a) minimum velocity = 0.005 m/s **(b) minimum velocity = 0.05 m/s**

Figure 7 - Flow channel for Δγ = 0 J/m² at T = 2.5s

5 WALL PRESSURES

Wall pressures from the DEM simulations have been determined using a spatial averaging method for the silo wall where a segment length of 15D (where D is the particle diameter) spaced at 2D has been used. The instantaneous, spatially averaged data for both the left and right walls are presented in the following figures as points, while temporally averaged data for the same time step is presented as a solid line. Data have been temporally averaged at a sampling frequency of 10Hz. Comparisons made between the DEM data and that predicted by Janssen Theory are also included. The mobilized wall friction (Figure 8) has been measured as an average value of 0.4 during discharge and a value of 0.3 before discharge and these are used with the Janssen theory for comparison with the DEM results.

The DEM wall pressures before discharge are, for the most part, in strong agreement with the Janssen prediction when the average mobilized friction coefficient calculated for this timestep is used. The distribution is initially hydrostatic with a close match to the mean mobilized friction. The match diverges with height, suggesting that wall friction has only been slightly mobilized in this region. A closer match was noted when a wall friction value of 0.2 was utilised.

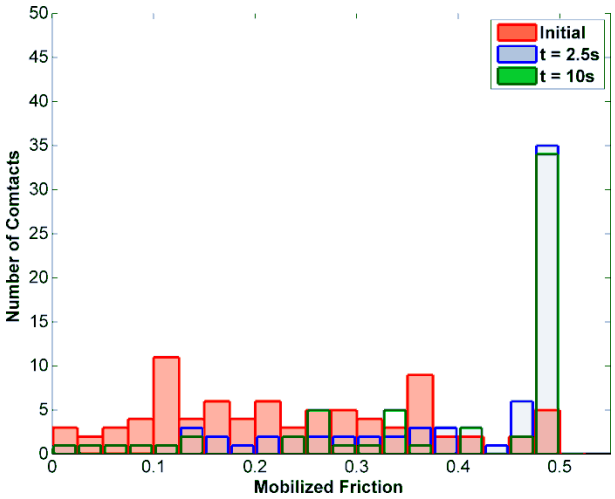

Figure 8 - Mobilized Friction for the cohesionless assembly (LHS) at various discharge times

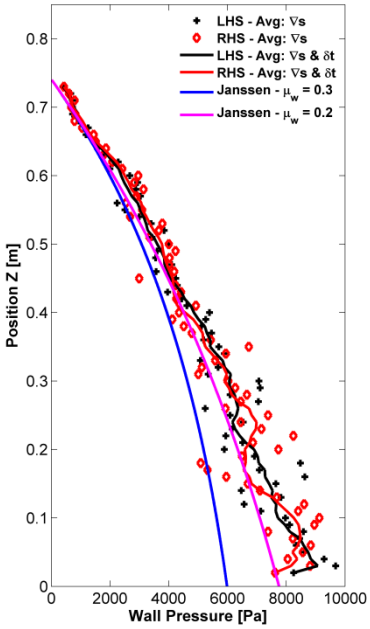

Figure 9 - Wall pressures before discharge

The wall pressure distribution for the cohesionless assembly, along with the internal horizontal and vertical stress are presented in Figure 10 and Figure 11.The wall pressures for each side are similar but not identical. Small variations in the flow channels lead to asymmetrical wall pressures during discharge. Higher wall pressures are known to exist where mass flow occurs and higher pressures can often be expected in the region of the effective transition [13]. This is also true for the DEM simulations which display an increased wall pressure (Figure 10a) in the region of approximately 0.2-0.4m on the left wall, whereas the wall pressure begins to drop from approximately 0.3m on the right wall. The internal horizontal stresses (Figure 10b) are significantly higher in this zone and also show high stress for a larger area on the left hand side. Significant arching occurs in the location of the effective transition where the flow mode changes from funnel to mass flow. The vertical stresses (Figure 10c) show significant vertical stress carried either side of the high velocity core flow channel transferred from the arching occurring around the effective transition into stagnant zones and silo base.

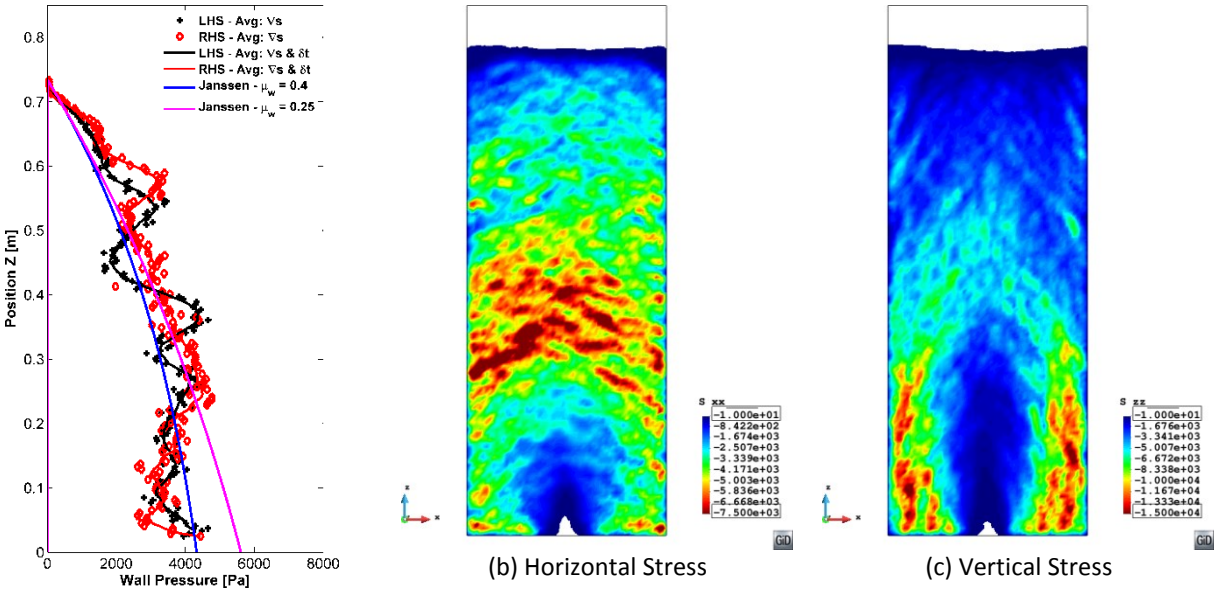

(a) Wall pressures (b) Horizontal Stress (c) Vertical Stress

Figure 10 – Wall pressure and internal stresses ($\Delta\gamma$ = 0 J/m²) at T = 1s

The same general trends are seen as flow progresses at T =2.5 sec in Figure 11, however the asymmetry in the flow channel has led to the highest wall pressure being observed on the right hand side at this time step. Again significant arching is noted around the effective transition and above it in the mass flow zone leading to higher wall pressures being observed here.

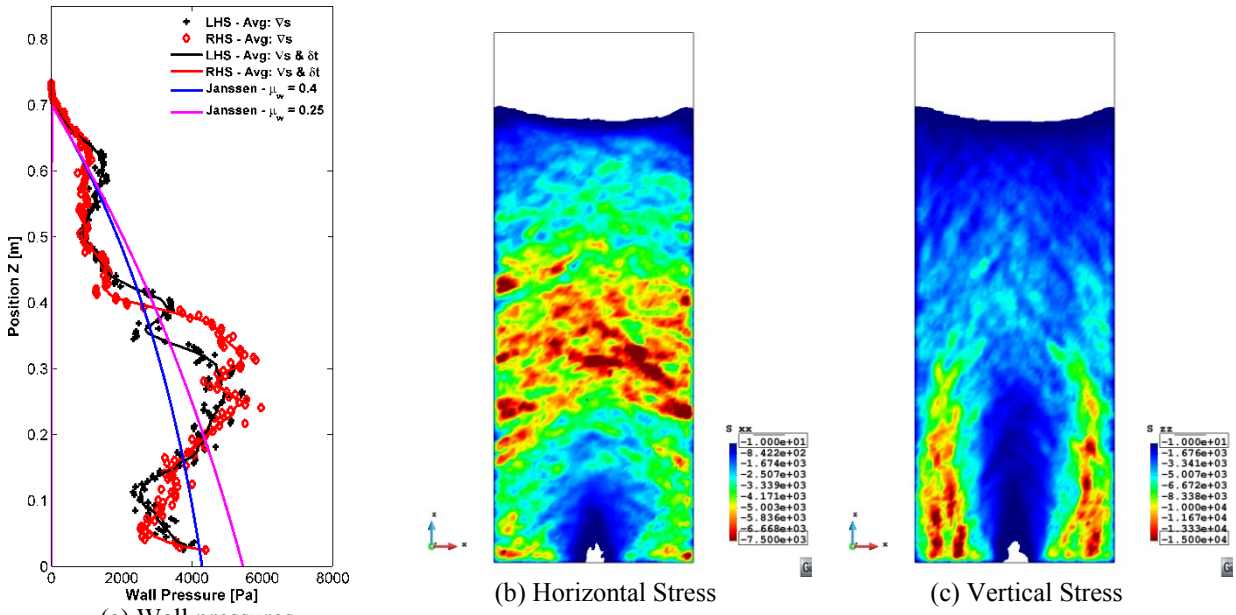

(a) Wall pressures (b) Horizontal Stress (c) Vertical Stress

Figure 11 – Wall pressure and internal stresses ($\Delta\gamma$ = 0 J/m²) at T = 2.5s

While no significant differences were noted in the observed flow patterns for increasing levels of contact adhesion during discharge lower discharge rates and longer time needed to reach a stable discharge rate were found. This is highlighted in Figure 12 where the wall

pressure distribution and internal stresses for the strongly cohesive assembly are presented. For this assembly a temporary cohesive arch formed between 0.5-1secs halting flow completely. Following the collapse of the arch the discharge rate slowly increases until a constant rate is developed at approximately 4s. The wall pressure distribution shows that in the upper section of the silo where there has been very little or no particle movement that the developed wall pressures are still very much similar to the static pressure distribution seen in Figure 9. In the lower half of the silo significantly reduced wall pressures are found as the cohesive solid begins to empty from the silo creating a high porosity flow channel before flow above the effective transition is fully developed.

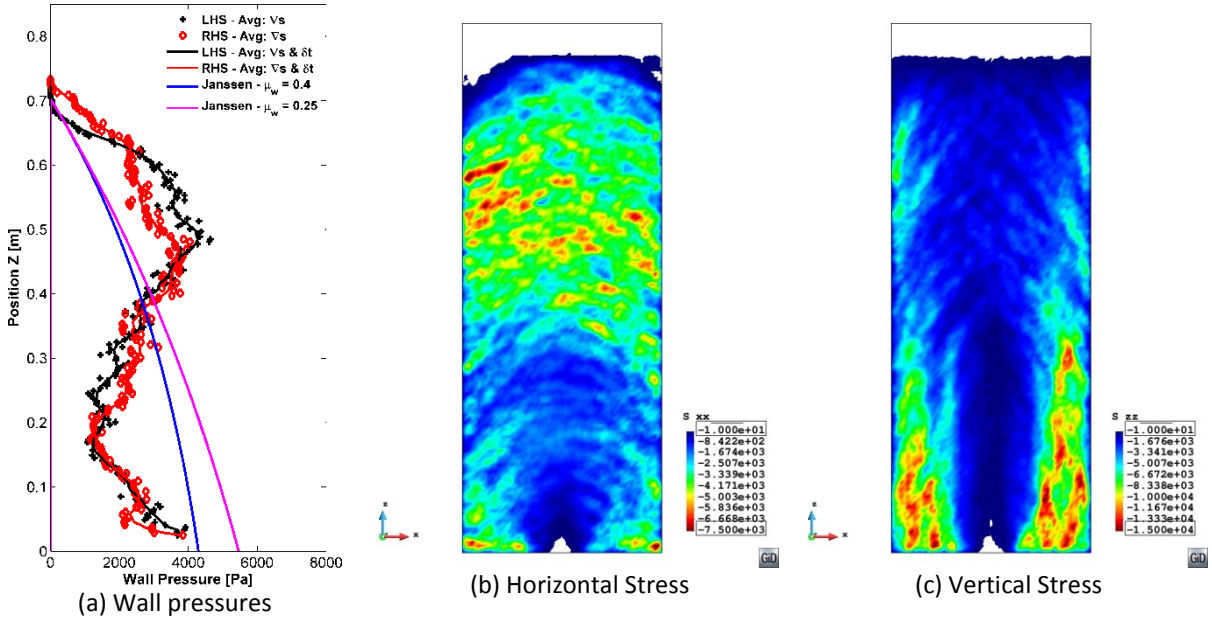

(a) Wall pressures (b) Horizontal Stress (c) Vertical Stress

Figure 12 – Wall pressure and internal stresses ($\Delta\gamma$ = 12.5 J/m²) at T = 2.5s

6 CONCLUSIONS

The effect of increasing levels of adhesion has been explored for a flat bottomed silo where the adhesion has been varied from cohesionless to extremely cohesive. The DEM simulations were found to capture the major phenomena occurring in silo flow including the various flow zones associated with a flat bottomed hopper: the effective transition and mass and funnel flow associated with a mixed flow pattern in the silo. The location of the effective transition height was identified at approximately H/W = 0.75-0.8 from a combination of the velocity profiles and the velocity contours in the silo. Above this mass flow was observed, with the velocity determined from the discharge rate and the velocity profile found to be in excellent agreement. A high velocity core flow zone was observed above the outlet where velocities were greater than1.25 V_{MF}.

The increase of adhesion in the silo was not found to significantly alter the flow patterns. However, a higher adhesion led to a reduced flow rate until the eventual blockage of the silo for the extremely cohesive case. The increase of adhesion also increases the probability of arching. Intermittent arching behaviour was noted in cases with higher levels of adhesion.

The wall pressures observed in the DEM model silo were found to be in good agreement

with the predicted behaviour with higher wall pressure observed above the effective transition where mass flow occurred. The wall pressures were sensitive to flow patterns during discharge. Minor variations in the flow channel can lead to asymmetry in wall pressures. The presence of adhesion did not lead to significantly different wall pressures, but reduced discharge rates.

ACKNOWLEDGEMENTS

The authors would like to thank EPSRC, LKAB and DEM Solutions Ltd for the funding and sponsorship. We are also grateful for the input and discussion with J. Sun of Edinburgh University, K. Tano and S.E. Forsmo of LKAB (Sweden) and G. Horrigmoe of Sweco Norge.

REFERENCES

[1] S. Luding, "Introduction to discrete element methods," *European Journal of Environmental and Civil Engineering*, vol. 12, no. 7–8, pp. 785–826, Aug. 2008.

[2] J. Tomas, "Adhesion of ultrafine particles—A micromechanical approach," *Chemical Engineering Science*, vol. 62, no. 7, pp. 1997–2010, Apr. 2007.

[3] O. R. Walton and R. L. Braun, "Viscosity, granular-temperature, and stress calculations for shearing assemblies of inelastic, frictional disks," *Journal of Rheology*, vol. 30, no. 5, pp. 949–980, 1986.

[4] J. P. Morrissey, "Discrete Element Modelling of iron ore fines to include the effects of moisture and fines," University of Edinburgh, 2013.

[5] R. Jones, "From Single Particle AFM Studies of Adhesion and Friction to Bulk Flow: Forging the Links," *Granular Matter*, vol. 4, no. 4, pp. 191–204, Feb. 2003.

[6] S. Luding, "Cohesive, frictional powders: contact models for tension," *Granular Matter*, vol. 10, no. 4, pp. 235–246, Mar. 2008.

[7] S. Luding, "Anisotropy in cohesive, frictional granular media," *Journal of Physics: Condensed Matter*, vol. 17, no. 24, pp. S2623–S2640, Jun. 2005.

[8] J. Munch-Andersen, "The Boundary Layer in Rough Silos," *Second International Conference on Bulk Materials Storage, Handling and Transportation: 1986; Preprints of Papers*, p. 160, 1986.

[9] J. Munch-Andersen, V. Askegaard, and A. Brink, *Silo model tests with sand. Bulletin No. 91*. Danish Building Research Institute., 1992, pp. 1–39.

[10] K. F. Zhang and J. Y. Ooi, "A kinematic model for solids flow in flat-bottomed silos," *Geotechnique*, vol. 48, no. 1998, pp. 545–553, 1998.

[11] W. A. Beverloo, H. A. Leniger, and J. Van de Velde, "The flow of granular solids through orifices," *Chemical Engineering Science*, vol. 15, pp. 260–269, 1961.

[12] M. E. Myers and M. Sellers, "Chemical engineering tripos. Part 2. Research Project Report," 1971.

[13] J. M. Rotter, *Guide for Economic Design of Circular Metal Silos*, Illustrate. Taylor & Francis, 2001, p. 235.